

Linking the atmospheric Pacific-South American mode with oceanic variability and predictability

Jiale Lou ^{1,2,5,6✉}, Terence J. O’Kane^{3,4} & Neil J. Holbrook ^{1,4}

While Pacific climate variability is largely understood based on El Niño-Southern Oscillation (ENSO), the North Pacific focused Pacific decadal oscillation and the basin-wide interdecadal Pacific oscillation, the role of the South Pacific, including atmospheric drivers and cross-scale interactions, has received less attention. Using reanalysis data and model outputs, here we propose a paradigm for South Pacific climate variability whereby the atmospheric Pacific-South American (PSA) mode acts to excite multiscale spatiotemporal responses in the upper South Pacific Ocean. We find the second mid-troposphere PSA pattern is fundamental to stochastically generate a mid-latitude sea surface temperature quadrupole pattern that represents the optimal precursor for the predictability and evolution of both the South Pacific decadal oscillation and ENSO several seasons in advance. We find that the PSA mode is the key driver of oceanic variability in the South Pacific subtropics that generates a potentially predictable climate signal linked to the tropics.

¹Institute for Marine and Antarctic Studies, University of Tasmania, Hobart, TAS, Australia. ²ARC Centre of Excellence for Climate System Science, University of Tasmania, Hobart, TAS, Australia. ³CSIRO Oceans and Atmosphere, Hobart, TAS, Australia. ⁴ARC Centre of Excellence for Climate Extremes, University of Tasmania, Hobart, TAS, Australia. ⁵Present address: Cooperative Institute for Research in the Environmental Sciences, University of Colorado Boulder, Boulder, CO, USA. ⁶Present address: Physical Sciences Laboratory, NOAA, Boulder, CO, USA. ✉email: jiale.lou@noaa.gov

Pacific decadal variability has been historically understood in terms of the North Pacific-focused Pacific decadal oscillation (PDO¹) and by the basin-scale interdecadal Pacific oscillation (IPO²). However, neither the PDO nor the IPO explicitly isolates the South Pacific contribution. Analogous to the PDO, the South Pacific decadal oscillation (SPDO^{3,4}) has been identified and described as the South Pacific centre of action contributing to the entire basin-wide Pacific decadal variability. Studies^{4,5} show that the SPDO can be viewed as a combination of different dynamical processes operating on different timescales. Those processes include the atmospheric forcing, tropical El Niño–Southern Oscillation (ENSO) teleconnections, and the internal oceanic dynamics. Importantly, the atmospheric forcing associated with the Pacific–South American pattern 1 (PSA1) has been identified as the main stochastic driver of the SPDO⁴ (cf. Fig. 1 (left)). ENSO has been shown to impact extratropical variability via the atmospheric bridge⁶ and oceanic pathways⁷.

Recent studies point out that extratropical ocean dynamics can feed back to the tropical Pacific via a sea surface temperature (SST) quadrupole pattern⁸ or a South Pacific meridional mode^{9–11}. Despite showing similar spatial patterns^{8,9}, the dynamical connections between the quadrupole pattern and the meridional mode in the South Pacific remain unclear. These oceanic processes act as extratropical precursors that might potentially guide the predictability and evolution of ENSO.

In this study, we propose a paradigm for South Pacific climate variability whereby the atmospheric eastward-propagating PSA mode pair can excite extratropical South Pacific Ocean responses on multiple time scales ranging from seasonal to decadal. Although the South Pacific Ocean responds to fast-varying atmospheric forcing on distinct timescales, the resultant spatial SST features remain difficult to distinguish from the background state. This suggests that the characterisation and identification of predictable signals, and their sources, require careful separation of

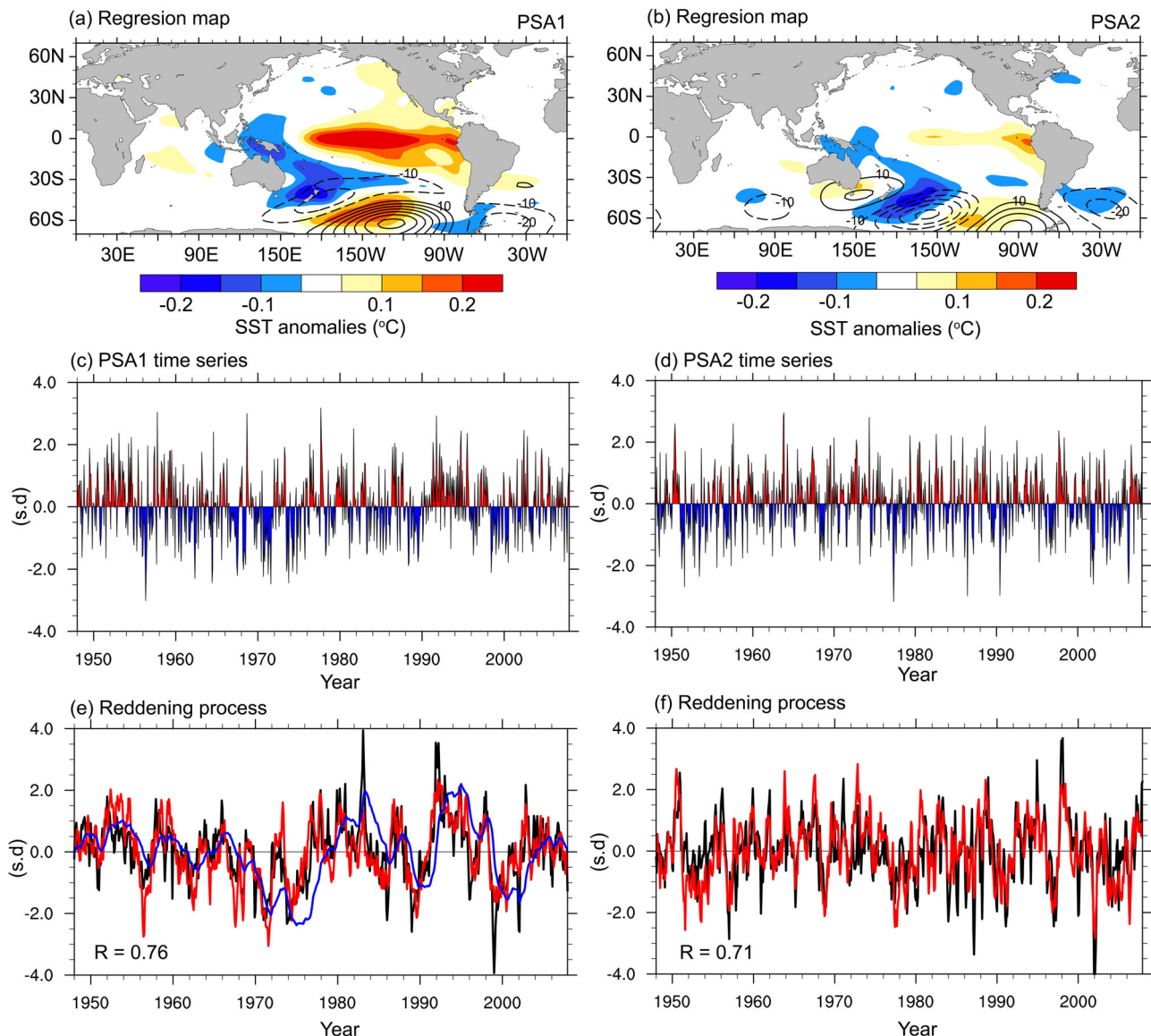


Fig. 1 Atmospheric forcing of the leading two SST modes in the South Pacific Ocean. The PSA1 (a) and PSA2 (b) patterns are obtained by regressing the monthly near-global Z500 anomalies (NCEP–NCAR; contour) and monthly SST anomalies (ACCESS–O; shade) onto the PSA1 and PSA2 time series, respectively. **c, d** The corresponding normalised PSA1 and PSA2 time series. **e, f** The time series of the leading two SST modes of variability in the South Pacific Ocean (ACCESS–O; black) are reconstructed (red) using an AR1 model forced by the PSA1 and PSA2 time series. The blue curve in (e) indicates the second integration forced by the SST SPDO time series. The units are in standard deviations (s.d.). The significance of the temporal correlations is estimated taking account of the effective number of degrees of freedom due to serial correlation⁴⁸.

the climate signal and relevant noise processes. This remains a necessary but challenging problem.

Results and discussion

The atmospheric Pacific–South American mode. The PSA mode is represented by an eastward-propagating wave train extending from eastern Australia to Argentina, characterised in mid-tropospheric geopotential height by two invariant empirical orthogonal function (EOF) patterns with associated principal component (PC) time series (PSA1 and PSA2; see Fig. S1) whose phases are nearly in quadrature with each other and whose explained variances are of nearly equal amplitude^{12,13}. In combination, they produce the single propagating PSA mode. The PSA mode is known to strongly influence the Antarctic cryosphere¹⁴, wind and significant wave heights across the Southern Hemisphere oceans, and the South American monsoon system including rainfall¹⁵ and weather and climate extremes over Brazil¹⁶.

The respective PSA1 pattern has been widely recognised as being highly correlated with ENSO, where previous studies argue that it results in part as an atmospheric response to ENSO^{15,17,18}. While regression analysis shows that there is indeed a very close relationship between PSA1 and ENSO (Fig. 1a), the origin of this relationship remains an active area of research^{19,20}. Meanwhile, the connection between the atmospheric PSA2 and tropical SST variability is less clear. Reference¹⁵ argues that PSA2 is responsible for the quasi-biennial component of ENSO (Fig. 1b). Although ENSO–PSA correlations are widely documented, the processes by which ENSO and the PSA mode are dynamically connected, and, in particular, how the PSA mode feeds back to the tropics, remain unclear.

Diverse views exist on the mechanisms that link the atmospheric PSA mode with ENSO. Some studies^{15,17,21,22} argue that the ENSO–PSA connection is directly linked via atmospheric Rossby wave propagation. However, other studies^{20,23,24} point out that synoptic-scale Rossby waves are primarily generated and trapped locally within the Southern Hemisphere subtropical and polar jet streams. Unlike the teleconnection between the Madden–Julian oscillation and North Atlantic oscillation²⁵, there is little direct dynamical evidence in terms of Rossby wave source or wave activity flux^{19,20,26} to suggest that poleward propagating large-scale tropical Pacific Rossby waves, potentially initiated by ENSO variability, teleconnect the PSA to ENSO. Even if sufficient Rossby wave sources were to be generated in the equatorial Pacific, ray tracing theory and wave activity flux calculations make it readily apparent that they are blocked by a reflecting barrier associated with the presence of the subtropical jet, and low latitude wave breaking, from propagation to the midlatitudes. Instead, ref. 27 argues that the PSA mode is linked to ENSO via a direct modulation of the midlatitude jets by the thermal winds generated by tropical convection that is highly correlated with ENSO. This indirectly influences the interannual variability of coherent synoptic features forming within these midlatitude waveguides where local Rossby wave sources are prevalent.

Oceanic signal driven by the PSA mode. Analysis of South Pacific SST shows that the first two modes of SST variability, referred to as the SPDO^{3,4} and South Pacific SST quadrupole pattern⁸ (Fig. S2), are primarily driven by the variability associated with the atmospheric PSA1 and PSA2 patterns (Fig. 1e, f). Using a univariate first-order autoregressive (AR1) model^{28,29}, we found that the integrated atmospheric PSA1 and PSA2 variability could explain a significant fraction of the variance of the first two SST modes in the South Pacific Ocean (Fig. 1e, f; $R = 0.76$ and

0.71 , respectively; significant at $>99\%$ level; see the “Methods” section for details).

A second integration of the AR1 model (following a similar approach to refs. 4,30)—with the first integration being from the atmosphere to the surface ocean, and the second integration from the surface ocean to the subsurface ocean—reveals that the leading SST mode is further reddened by the extratropical upper ocean (Fig. 1e). The integrated SPDO signal (blue curve in Fig. 1e) resembles the time evolution of the leading vertically averaged temperature (VAT) mode through the upper 300 m of the ocean (see the “Methods” section), with a temporal correlation of $R = 0.88$ (statistically significant at the 99% level). To first order, we conclude that the South Pacific Ocean integrates the fast-varying atmospheric “noise” forcing to produce a “reddened” oceanic signal, with a pronounced increase in the amplitude of the spectrum at low frequencies and decreased amplitude at high frequencies, where the main potentially predictable signal is generated on the time scales of the ocean dynamics.

Oceanic noise driven by the PSA mode. The extratropical South Pacific not only responds via reddening processes to the fast-varying atmosphere but also via coherence resonances³¹. Specifically, the forcing due to coherent synoptic-scale disturbances in the atmosphere associated with the PSA imprints onto the surface ocean further enhancing internal SST variability at its preferred frequency. To examine this mechanism, we generalised the univariate AR1 model to a higher-dimensional multivariate field through the inclusion of SST anomalies in the tropical and South Pacific oceans using a linear inverse model³² (LIM; see “Methods” section). Previous studies have shown that the tropical and South Pacific oceans can be approximated as a stochastically forced linear system, where different dynamical processes are represented by distinct damping time scales via the decomposition of the LIM^{5,32–35}.

Figure 2 shows the fastest damped SST mode pair with a damping time scale of two months. This pair of complex patterns (Fig. 2a, b) constitutes a single propagating wave train with a complete cycle of 26 months. Along with the propagating features, the spatial patterns of the fastest damped modes also bear a strong resemblance to the atmospheric PSA1 and PSA2 patterns. Projecting the corresponding time series of the real and imaginary components of the fastest damped mode onto the monthly 500 hPa geopotential height (Z500) anomalies produces regression maps (Fig. 2c, d) that closely resemble the atmospheric PSA1 and PSA2 with spatial correlations of 0.74 and 0.69 (statistically significant at the 95% level), respectively, in the South Pacific region. This suggests that the high-frequency atmospheric PSA fluctuations can excite SST modes whose frequencies are subject to the atmospheric drivers. In contrast to the reddening processes that act to excite the potentially predictable low-frequency ocean signal, the pair of most damped SST modes are correlated with the atmospheric PSA forcing that acts as noise on the SST system.

The optimal growth and extratropical precursor. Previous studies have extensively discussed the tropical and extratropical precursors of ENSO^{8,10,32,36,37}. Despite there being little direct evidence, in terms of atmospheric dynamics, to show that the atmospheric PSA mode can directly modulate ENSO evolution in the tropics²⁷, the indirect influence has nevertheless been widely identified in both observations¹¹ and model simulations^{36,38} via the “atmosphere → extratropical ocean → tropical ocean” pathway. One way in which this indirect influence may occur is through a “seasonal footprinting” mechanism³⁹, where the

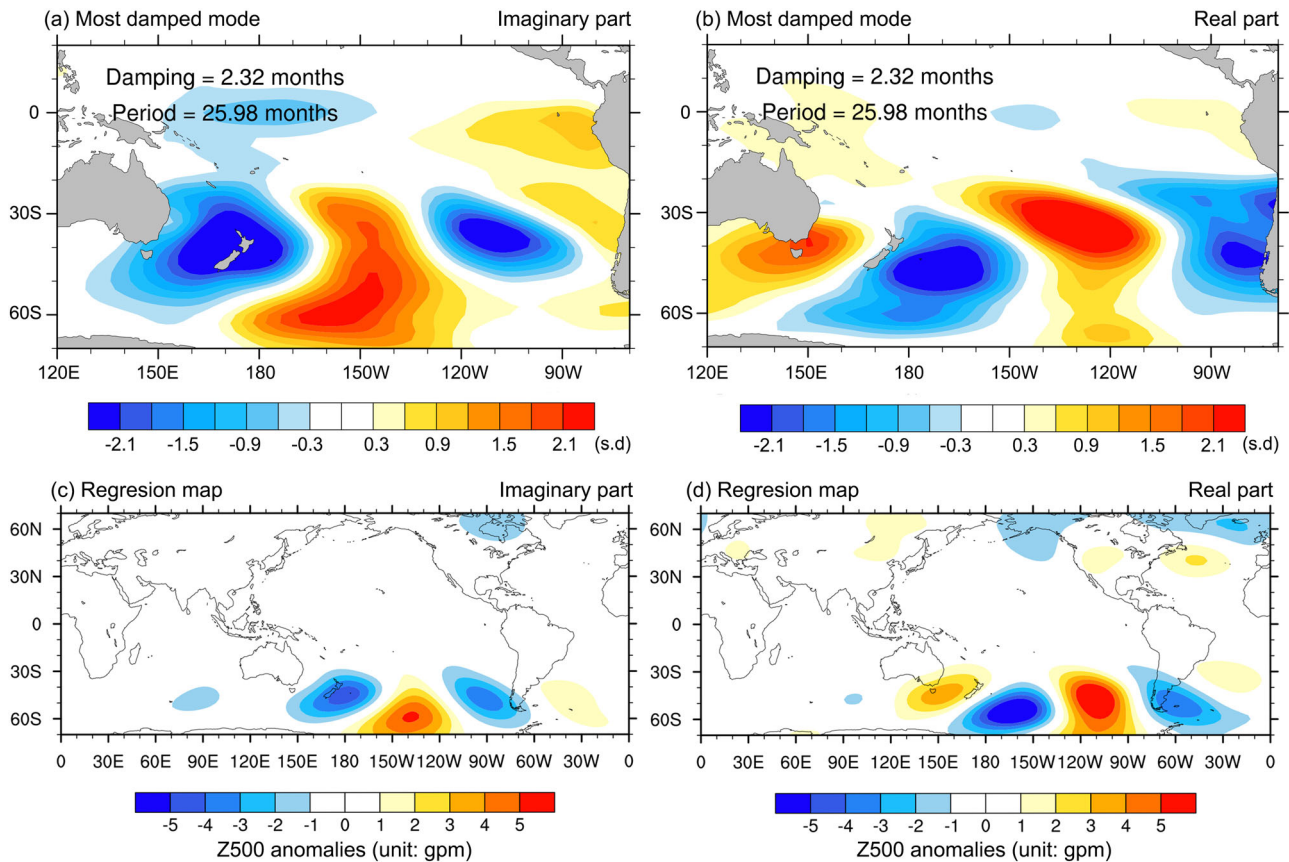


Fig. 2 The fastest damped SST modes. The imaginary (a) and real (b) parts of the fastest damped SST modes are obtained using a reduced-order linear inverse model (see the text for details). The pair of SST modes shown has the fastest damping time scale of 2.3 months. The maps are obtained by regressing the monthly Z500 anomalies (NCEP-NCAR) onto the time series of the imaginary (c) and real (d) parts of the fastest damped modes.

atmospheric forcing drives an extratropical anomalous SST “footprint” in the boreal spring, which persists through the boreal summer, and sustains wind stress anomalies in the tropics that are crucial to initiate ENSO events.

The LIM approach enables an objective determination of the optimal initial perturbations that maximise, for example, ENSO and SPDO growth. This provides an ideal framework through which to investigate the dynamical precursors and predictability of the peak phases of ENSO and the SPDO. Unlike lead-lag correlations that have been widely applied to identify ENSO precursors^{8,9,11}, the LIM represents a multivariate linear stochastically forced model and provides a dynamical approximation (see “Methods” section) that satisfies conditionally causal⁴⁰ relationships between the optimal precursors and their peak phases.

The interference between the non-normal damping SST modes can give rise to a transient amplification of the variance of the deterministic SST system at a preferred temporal growth scale. Such transient amplification is useful in sampling and interpreting errors in initial conditions⁴¹ and explains the actual variance growth in the system³². Transient amplification of monthly tropical and South Pacific SST anomalies allows a specific set of initial perturbations to develop into the peak phases that are found to exist at 6- to 10-month lead times^{5,9,32,33,42}. Our LIM experimental results show that the optimal growth time of SST anomalies in the tropical and South Pacific oceans (see “Methods” section) is 9 months. These results imply the existence of linear growth events that act to maximise ENSO and SPDO development leading to enhanced predictability if the initial perturbations can be sufficiently well specified.

The spatial patterns of the initial SST perturbations in the tropical Pacific and South Pacific are shown in Fig. 3a, c, respectively. These initial patterns co-evolve over nine months into the optimal final peak phases in Fig. 3b, d, which are closely associated with ENSO and the SPDO with pattern correlations of 0.99 and 0.97 (statistically significant at the 99% level), respectively. The tropical ENSO precursor (Fig. 3a) has been discussed in the previous studies^{32,33,37,43} and may be associated with the recharge–discharge mechanism as first described by Jin⁴⁴. The extratropical precursor (Fig. 3c) resembles a quadrupole structure similar to the second South Pacific SST mode with the pattern correlation of 0.85 (significant at the 95% level). The initial and final spatial patterns (Fig. 3c, d) were projected onto the monthly SST anomalies to reconstruct the time series. The reconstructed time series of the optimal initial perturbations and final peak phases in the South Pacific (Fig. 3e, f) are highly correlated with the second and first South Pacific SST modes with temporal correlations of 0.86 and 0.98 (statistically significant at the 99% level), respectively. This suggests that the South Pacific quadrupole SST pattern, which is primarily driven by the atmospheric PSA2, is the optimal local (linear) precursor that maximises the SPDO growth. Given the almost synchronous features between ENSO and the SPDO^{3,4}, these results imply that the extratropical SST precursor of ENSO is also related to the quadrupole SST pattern in the South Pacific Ocean. Our results support the “seasonal footprinting” mechanism whereby the atmospheric PSA2 excites the South Pacific quadrupole SST anomalies, which then persist through the boreal summer to guide ENSO growth.

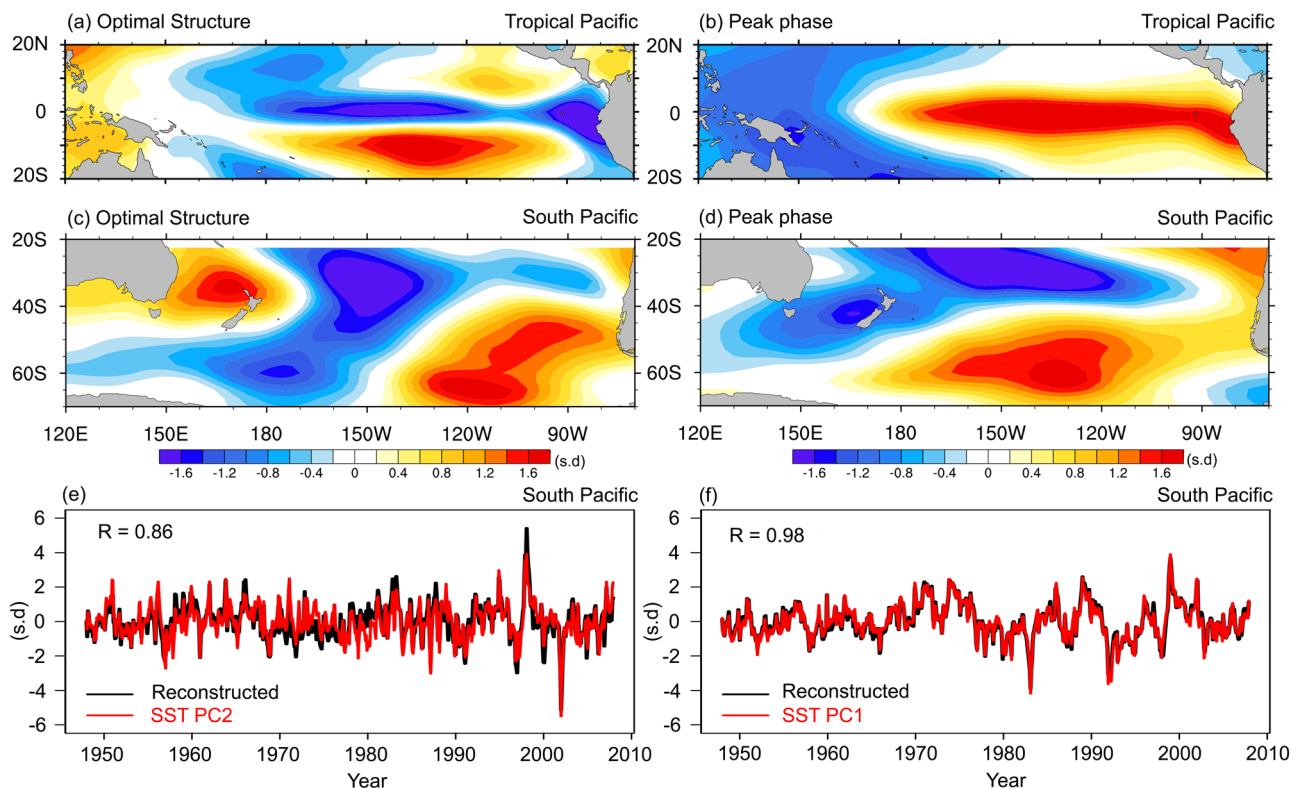


Fig. 3 The optimal evolution of the tropical and South Pacific SST. The optimal initial structures in the **a** tropical Pacific and **c** South Pacific are obtained using a linear inverse model (see the text for details), which linearly co-evolve over 9 months into their peak phases in the **b** tropical Pacific and **d** South Pacific. The spatial patterns shown in **(a–d)** are normalised according to the variance in each domain. The reconstructed time series of the **e** optimal initial structure and **f** peak phase in the South Pacific (black) are compared with the time series of the leading two South Pacific SST modes (red).

A paradigm for South Pacific climate variability and predictability. Figure 4 summarises the atmospheric PSA mode and its South Pacific Ocean responses based on the combined results from the AR1 and LIM investigations. Our results suggest that the eastward-propagating PSA mode provides an important source of atmospheric forcing to excite the extratropical South Pacific Ocean responses operating on multiple time scales via reddening processes and coherence resonances. To first order, the close relationships between the integrated PSA1 and PSA2 patterns and the leading South Pacific SST modes support the general concept that fast atmospheric variations are a critically important excitation source of low-frequency oceanic variability. The leading integrated subsurface temperature mode, that resembles the spatial pattern of its SST counterpart, can be regarded as a cumulative response to atmospheric PSA1 forcing. That is, the inclusion of extratropical subsurface processes further reddens the SST variations thereby enhancing the most persistent and potentially predictable signal. Furthermore, the atmospheric PSA1 and PSA2 patterns can excite SST variations via coherence resonances such that the resultant fastest damping SST modes are slaves to the atmospheric forcing but synchronised to the spatiotemporal features of the real and imaginary components of the propagating PSA.

The extratropical SST precursor of ENSO and SPDO growth is strongly associated with the South Pacific quadrupole SST pattern. The set of initial conditions related to this quadrupole pattern can optimally determine how the SST anomalies will evolve along its deterministic (linear) trajectory and lead to the SPDO and ENSO peaks over the following nine months, and from which the linear predictability intrinsic to the SST system can be inferred. While the influence of the atmospheric PSA mode on tropical SST variability is less apparent than the

influence of the tropical SST variability on the PSA mode^{8,20,27}, our results indicate that the South Pacific quadrupole SST pattern acts as an oceanic bridge that links the atmospheric PSA forcing to ENSO dynamics centred in the tropics, and represents the most probable pathway for midlatitude atmospheric variability to influence tropical SST via an indirect “seasonal footprinting” mechanism. Although the actual observed nonlinear dynamics are more complicated than the tangent linear dynamics that form the basis of the LIM propagator, the proposed paradigm provides a mechanistic framework to understand the dynamics and predictability of South Pacific climate variability and to interpret extratropical atmospheric drivers and the oceanic responses on multiple time scales.

Methods

The reanalysis data used here were monthly detrended anomalies of the 500 hPa geopotential heights (Z500) from the National Centres for Environmental Prediction/National Centre for Atmospheric Research (NCEP-NCAR)⁴⁵. The monthly detrended SST anomalies were generated using an atmosphere-forced ocean model, the Australian Community Climate and Earth-System Simulator-Ocean (ACCESS-O). The ACCESS-O is forced by observed atmospheric fields from the Coordinated Ocean–Ice Reference Experiments (CORE; 1948–2007)⁴⁶. The model configuration is described in ref. ⁴⁷. The original 360×300 tripolar ACCESS-O model grid has been remapped to a regular $2.5^\circ \times 2.5^\circ$ grid. The reanalysis data and model simulations were linearly detrended at each grid point, with monthly anomalies calculated by removing the climatological monthly mean.

The atmospheric PSA1 and PSA2 patterns were defined by computing the second and third empirical orthogonal functions/principal components (EOFs/PCs) of the monthly Z500 anomalies in the Southern Hemisphere, respectively, which explain 11.2 and 8.3% of the total variance. The leading two South Pacific SST modes, which are referred to as the South Pacific decadal oscillation (SPDO) and the South Pacific quadrupole SST pattern, were obtained by computing the first and second EOFs/PCs of the monthly SST anomalies in the South Pacific Ocean domain from $(20^\circ\text{S}–70^\circ\text{S}; 120^\circ\text{E}–60^\circ\text{W})$, and explain 19.0 and 9.6% of the total variance. The subsurface temperature variability was characterised by spatiotemporal variations of vertically averaged temperatures (VAT) through the

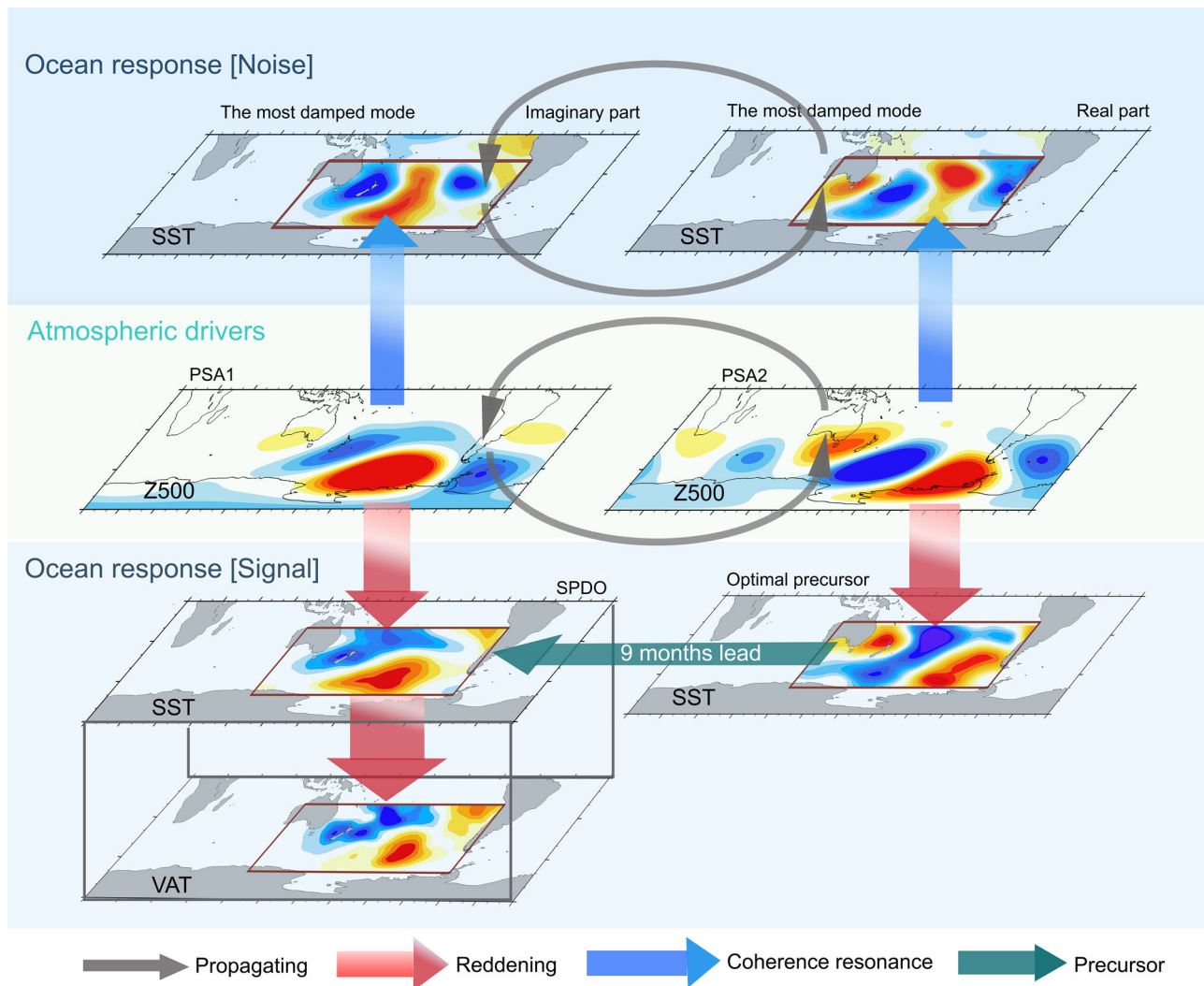


Fig. 4 Schematic of the paradigm for South Pacific Ocean variability and predictability. The top panels are the same as shown in Fig. 2a and b indicating the fastest damped mode pair. The middle panels are the second and third modes of the monthly Z500 anomalies (NCEP-NCAR) in the southern hemisphere. The left panels of the bottom layer are the leading EOF modes of the monthly SST anomalies and VAT anomalies in the South Pacific Ocean, respectively. The right panel of the bottom layer is the same as shown in Fig. 3c indicating the optimal precursor of the SPDO (illustrated by the green arrow). Red arrows indicate reddening processes. Blue arrows indicate coherence resonances. Grey arrows indicate the propagating features of the corresponding modes.

upper 300 m of the ocean, which includes the mixed layer and thermocline across most regions. The subsurface SPDO is derived from the first EOF/PC of the VAT in the South Pacific Ocean (20°S–70°S; 120°E–60°W) and explains 19.8% of the total variance. Statistical significance tests of the correlation coefficients calculated in this study took account of the effective number of degrees of freedom due to serial correlation in the time series, following the method of ref. 48.

The oceanic reddening response to atmospheric PSA forcing was quantified using a doubly integrated first-order autoregressive (AR1) model. A univariate AR1 model can be written as

$$\frac{dx}{dt} = lx + \xi, \quad (1)$$

where x is a time series and $-1/l$ is associated with the damping time scale. This univariate AR1 process only has one degree of freedom and is unable to oscillate when the damping coefficient l is positive⁴⁹. Predictability of the time series x is largely limited by the damping scale $-1/l$. ξ in Eq. (1) represents a high-frequency noise forcing term.

The optimal damping time scales are 6 months and 5 months, respectively, when the time series of the PSA1 and PSA2 patterns were specified as the atmospheric forcing of the first two South Pacific SST modes in the first AR1 integration from the atmosphere to the surface ocean. In the second integration from the surface ocean to the subsurface ocean, the optimal damping time scale is 15 months when the time series of the SST SPDO was specified as the forcing of the leading South Pacific VAT mode.

The pair of fastest damped noise mode and optimal initial perturbations were estimated using a generalised AR1 model, here referred to as the linear inverse model (LIM)³², or alternatively termed principal oscillation pattern (POP) analysis⁴⁹. The LIM can be written in the form of a linear stochastic differential equation:

$$\frac{d\mathbf{X}}{dt} = \mathbf{L}\mathbf{X} + \xi \quad (2)$$

where the evolution of the state vector \mathbf{X} can be expressed as the sum of the deterministic dynamics, $\mathbf{L}\mathbf{X}$, that constitute “slow” processes and the stochastic forcing term, ξ , that constitutes “fast” processes. In this study, we defined the model state vector \mathbf{X} as

$$\mathbf{X} = \begin{bmatrix} \text{SST}_{\text{TP}} \\ \text{SST}_{\text{SP}} \end{bmatrix}, \quad (3)$$

where we considered monthly SST anomalies from the tropical Pacific (i.e., SST_{TP} in the region 20°S–20°N, 120°E–60°W) and South Pacific Ocean (i.e., SST_{SP} in the region 22.5°S–70°S, 120°E–60°W). We retained the leading 4 tropical Pacific and 6 South Pacific SST EOFs/PCs in the LIM to reduce the spatial degrees of freedom and ensure linearity and stability of the SST system. The robustness of the LIM has been demonstrated in the refs. 5,50, showing that the choices of using the leading 10–16 EOFs/PCs to construct the state vector \mathbf{X} and the different combinations of the leading EOFs/PCs used from the different regions give similar results.

The dynamical operator \mathbf{L} in Eq. (2) encapsulates the evolution of the state vector \mathbf{X} and can be estimated from

$$\mathbf{L} = \tau_0^{-1} \ln [\mathbf{C}(\tau_0)\mathbf{C}(0)^{-1}], \quad (4)$$

where $\mathbf{C}(\tau_0)$ and $\mathbf{C}(0)$ are the time-lagged and zero-lagged (cross-)covariance matrices of the state vector \mathbf{X} . That is, $\mathbf{C}(\tau_0) = \langle \mathbf{X}(t + \tau_0)\mathbf{X}^T(t) \rangle$ and $\mathbf{C}(0) = \langle \mathbf{X}(t)\mathbf{X}^T(t) \rangle$, where the angle brackets here denote an ensemble average or a time average over all t for variables with stationary statistics. Here, $\tau_0 = 1$ month was used to ensure the stability of the LIM. Previous studies^{5,50} examined the sensitivity of using different choices of τ_0 to estimate the dynamical operator \mathbf{L} , finding that the LIM is insensitive to τ_0 ranging from 1 month to 6 months.

For a system described by Eq. (2), the most probable evolution at time $t + \tau$ can be determined by

$$\mathbf{X}(t + \tau) = \mathbf{G}(\tau)\mathbf{X}(t) = e^{\mathbf{L}\tau}\mathbf{X}(t), \quad (5)$$

given a state vector $\mathbf{X}(t)$.

The damping modes can then be diagnosed by applying eigen-decomposition to the dynamical operator \mathbf{L} (i.e., $\mathbf{L}\mathbf{p} = \lambda\mathbf{p}$). Since the \mathbf{L} matrix is not symmetric, some or all of its eigenvalues λ and eigenvectors \mathbf{p} are complex. The damping time scales $-1/\sigma$ and/or the oscillatory periods $2\pi/\omega$ of the damping modes can be directly estimated from the corresponding eigenvalues $\lambda = \sigma + i\omega$, where σ and ω are the real and imaginary parts of λ , respectively. In this study, the pair of complex damping modes that have the fastest damping time scale has been discussed.

The transient growth over any time interval τ can be written as the norm of the final state $\mathbf{X}(t)$ divided by the norm of the initial state $\mathbf{X}(0)$:

$$\gamma^2 = \frac{\|\mathbf{X}(t)\|^2}{\|\mathbf{X}(0)\|^2} = \frac{\mathbf{X}^T(t)\mathbf{X}(t)}{\mathbf{X}^T(0)\mathbf{X}(0)} = \frac{\mathbf{X}^T(0)\mathbf{G}^T(\tau)\mathbf{G}(\tau)\mathbf{X}(0)}{\mathbf{X}^T(0)\mathbf{X}(0)}. \quad (6)$$

The optimal growth that maximises the amplification of the variance can be estimated as the leading eigenvalue γ_1^2 of $\mathbf{G}^T(\tau)\mathbf{G}(\tau)$. The leading eigenvalues at different time intervals (i.e., $\gamma_1^2(\tau)$) then form a trajectory that indicates the modal interferences and variance changes of the system in the absence of stochastic forcing. Since the dynamical operator of the LIM is nonnormal (i.e., $\mathbf{L}^T \neq \mathbf{L}\mathbf{L}^T$), it allows the resultant damping modes to interact with each other and contribute to the transient amplification of the variance without the presence of stochastic forcing. This provides a perspective to, for example, interpret errors in the initial conditions and understand the error growth of the system. In the present LIM, the largest transient amplification of the SST variance was found at 9 months.

The optimal precursor indicates the initial condition that maximises the growth of the state vector over a specified time interval τ ($\tau = 9$ months in this case). The optimal precursor is derived as the corresponding leading eigenvector of $\mathbf{G}^T(\tau)\mathbf{G}(\tau)$ when $\tau = 9$ months is specified.

Data availability

The atmospheric data used in this work are freely available from <https://psl.noaa.gov/data/gridded/data.ncep.reanalysis.pressure.html>. The ACCESS-O model outputs and the AR1 and LIM codes used in this work are available at the Zenodo open data repository (<https://doi.org/10.5281/zenodo.5516236>).

Received: 30 June 2021; Accepted: 30 September 2021;

Published online: 21 October 2021

References

- Mantua, N. J. & Hare, S. R. The Pacific decadal oscillation. *J. Oceanogr.* **58**, 35–44 (2002).
- Power, S. et al. Inter-decadal modulation of the impact of ENSO on Australia. *Clim. Dynam.* **15**, 319–324 (1999).
- Chen, X. & Wallace, J. M. ENSO-like variability: 1900–2013*. *J. Climate* **28**, 9623–9641 (2015).
- Lou, J., Holbrook, N. J. & O’Kane, T. J. South Pacific decadal climate variability and potential predictability. *J. Climate* **32**, 6051–6069 (2019).
- Lou, J., O’Kane, T. J. & Holbrook, N. J. A linear inverse model of tropical and South Pacific seasonal predictability. *J. Climate* **33**, 4537–4554 (2020).
- Taschetto, A. S. et al. ENSO atmospheric teleconnections. In *El Niño Southern Oscillation in a changing climate* (eds. McPhaden, M. J., Santoso, A. & Cai W.) 309–335 (Wiley, 2020).
- Sprintall, J. et al. ENSO oceanic teleconnections. In *El Niño Southern Oscillation in a changing climate* (eds. McPhaden, M. J., Santoso, A. & Cai W.) 337–359 (Wiley, 2020).
- Ding, R., Li, J. & Tseng, Y.-H. The impact of South Pacific extratropical forcing on ENSO and comparisons with the North Pacific. *Clim. Dynam.* **44**, 2017–2034 (2015).
- Zhao, Y. & Di Lorenzo, E. The impacts of extra-tropical ENSO precursors on tropical Pacific decadal-scale variability. *Sci. Rep.* **10**, 3031 (2020).
- Zhang, H., Clement, A. & Di Nezio, P. The South Pacific meridional mode: a mechanism for ENSO-like variability. *J. Climate* **27**, 769–783 (2014).
- You, Y. & Furtado, J. C. The role of South Pacific atmospheric variability in the development of different types of ENSO. *Geophys. Res. Lett.* **44**, 7438–7446 (2017).
- Lau, K. M., Sheu, P. J. & Kang, I. S. Multiscale low-frequency circulation modes in the global atmosphere. *J. Atmos. Sci.* **51**, 1169–1193 (1994).
- Echevarria, E. R. et al. Influence of the Pacific-South American modes on the global spectral wind-wave climate. *J. Geophys. Res. Oceans* **125**, e2020JC016354 (2020).
- Irving, D. & Simmonds, I. A new method for identifying the Pacific-South American pattern and its influence on regional climate variability. *J. Climate* **29**, 6109–6125 (2016).
- Mo, K. C. & Paegle, J. N. The Pacific-South American modes and their downstream effects. *Int. J. Climatol.* **21**, 1211–1229 (2001).
- Rehbein, A. et al. Severe weather events over southeastern Brazil during the 2016 dry season. *Adv. Meteorol.* **2018**, 4878503 (2018).
- Karoly, D. J. Southern Hemisphere circulation features associated with El Niño–Southern Oscillation events. *J. Climate* **2**, 1239–1252 (1989).
- Cai, W. et al. Climate impacts of the El Niño–Southern Oscillation on South America. *Nat. Rev. Earth Environ.* **1**, 215–231 (2020).
- Karoly, D. J., Plumb, R. A. & Ting, M. Examples of the horizontal propagation of quasi-stationary waves. *J. Atmos. Sci.* **46**, 2802–2811 (1988).
- Li, X. et al. A Rossby wave bridge from the tropical Atlantic to West Antarctica. *J. Climate* **28**, 2256–2273 (2015).
- Renwick, J. A. & Revell, M. J. Blocking over the South Pacific and Rossby wave propagation. *Mon. Weather Rev.* **127**, 2233–2247 (1999).
- Cai, W. et al. Teleconnection pathways of ENSO and the IOD and the mechanisms for impacts on Australian rainfall. *J. Climate* **24**, 3910–3923 (2011).
- Ambrizzi, T. & Hoskins, B. J. Stationary Rossby-wave propagation in a baroclinic atmosphere. *Q. J. R. Meteorol. Soc.* **123**, 919–928 (1997).
- Ambrizzi, T., Hoskins, B. J. & Hsu, H.-H. Rossby wave propagation and teleconnection patterns in the austral winter. *J. Atmos. Sci.* **52**, 3661–3672 (1995).
- Lin, H. & Brunet, G. Extratropical response to the MJO: nonlinearity and sensitivity to the initial state. *J. Atmos. Sci.* **75**, 219–234 (2018).
- O’Kane, T. J. et al. On the dynamics of persistent states and their secular trends in the waveguides of the Southern Hemisphere troposphere. *Clim. Dynam.* **46**, 3567–3597 (2015).
- O’Kane, T. J., Monselesan, D. P. & Risbey, J. S. A multiscale reexamination of the Pacific-South American pattern. *Mon. Weather Rev.* **145**, 379–402 (2017).
- Frankignoul, C. & Hasselmann, K. Stochastic climate models, Part II Application to sea-surface temperature anomalies and thermocline variability. *Tellus* **29**, 289–305 (1977).
- Hasselmann, K. Stochastic climate models Part I. Theory. *Tellus* **28**, 473–485 (1976).
- Di Lorenzo, E. & Ohman, M. D. A double-integration hypothesis to explain ocean ecosystem response to climate forcing. *Proc. Natl. Acad. Sci. USA* **110**, 2496–9 (2013).
- Pierini, S. Low-frequency variability, coherence resonance, and phase selection in a low-order model of the wind-driven ocean circulation. *J. Phys. Oceanogr.* **41**, 1585–1604 (2011).
- Penland, C. & Sardeshmukh, P. D. The optimal growth of tropical sea surface temperature anomalies. *J. Climate* **8**, 1999–2024 (1995).
- Capotondi, A. & Sardeshmukh, P. D. Optimal precursors of different types of ENSO events. *Geophys. Res. Lett.* **42**, 9952–9960 (2015).
- Newman, M. Interannual to decadal predictability of tropical and North Pacific sea surface temperatures. *J. Climate* **20**, 2333–2356 (2007).
- Penland, C. & Magorian, T. Prediction of Niño 3 sea surface temperatures using linear inverse modeling. *J. Climate* **6**, 1067–1076 (1993).
- Liguori, G. & Di Lorenzo, E. Separating the North and South Pacific meridional modes contributions to ENSO and tropical decadal variability. *Geophys. Res. Lett.* **46**, 906–915 (2019).
- Penland, C. & Matrosova, L. Studies of El Niño and interdecadal variability in tropical sea surface temperatures using a nonnormal filter. *J. Climate* **19**, 5796–5815 (2006).
- Zhang, H. et al. Equatorial signatures of the Pacific meridional modes: dependence on mean climate state. *Geophys. Res. Lett.* **41**, 568–574 (2014).
- Vimont, D. J., Wallace, J. M. & Battisti, D. S. The seasonal footprinting mechanism in the Pacific: implications for ENSO. *J. Climate* **16**, 2668–2675 (2003).
- Granger, C. W. J. Some recent development in a concept of causality. *J. Econom.* **39**, 199–211 (1988).
- Moore, A. M. & Kleeman, R. The dynamics of error growth and predictability in a coupled model of ENSO. *Q. J. R. Meteorol. Soc.* **122**, 1405–1446 (1996).
- Newman, M., Alexander, M. A. & Scott, J. D. An empirical model of tropical ocean dynamics. *Clim. Dynam.* **37**, 1823–1841 (2011).

43. Hu, S. & Fedorov, A. V. Exceptionally strong easterly wind burst stalling El Niño of 2014. *Proc. Natl. Acad. Sci. USA* **113**, 2005–2010 (2016).
44. Jin, F.-F. An equatorial ocean recharge paradigm for ENSO. Part I: Conceptual model. *J. Atmos. Sci.* **54**, 811–829 (1997).
45. Kalnay, E. et al. The NCEP/NCAR 40-year reanalysis project. *Bull. Am. Meteorol. Soc.* **77**, 437–472 (1996).
46. Griffies, S. M. et al. Coordinated Ocean-ice Reference Experiments (COREs). *Ocean Model.* **26**, 1–46 (2009).
47. O’Kane, T. J. et al. Storm tracks in the Southern Hemisphere subtropical oceans. *J. Geophys. Res. Oceans* **119**, 6078–6100 (2014).
48. Davis, R. E. Predictability of sea surface temperature and sea level pressure anomalies over the North Pacific Ocean. *J. Phys. Oceanogr.* **6**, 249–266 (1976).
49. von Storch, H. et al. Principal oscillation patterns: a review. *J. Climate* **8**, 377–400 (1995).
50. Lou, J., O’Kane, T. J. & Holbrook, N. J. A linear inverse model of tropical and South Pacific climate variability: optimal structure and stochastic forcing. *J. Climate* **34**, 143–155 (2021).

Acknowledgements

We want to thank the two reviewers for their constructive reviews which have helped to improve this manuscript. J.L. is grateful for a PhD scholarship provided by the ARC Centre of Excellence for Climate System Science (CE110001028), a University of Tasmania tuition fee scholarship, and a CSIRO-UTAS Quantitative Marine Science top-up scholarship [including support from the Australian Commonwealth Scientific Research Organisation (CSIRO) Postgraduate scheme]. Partial support for J.L. was also supplied by the US DOE (Grant 0000238382). T.J.O. was supported by the CSIRO Decadal Climate Forecasting Project (<https://research.csiro.au/dfp>). N.J.H. acknowledges funding support from the ARC Centre of Excellence for Climate Extremes (CE170100023) and the Australian Government National Environmental Science Programme Climate Systems Hub.

Author contributions

J.L. conceived the work, carried out the data analyses, and wrote most of the paper. T.J.O. supplied the ACCESS-O model outputs. T.J.O. and N.J.H. contributed to the interpretation of the model results and analysis, and also to the text.

Competing interests

The authors declare no competing interests.

Additional information

Supplementary information The online version contains supplementary material available at <https://doi.org/10.1038/s43247-021-00295-4>.

Correspondence and requests for materials should be addressed to Jiale Lou.

Peer review information *Communications Earth & Environment* thanks the anonymous reviewers for their contribution to the peer review of this work. Primary Handling Editors: Clara Orbe, Heike Langenberg. Peer reviewer reports are available.

Reprints and permission information is available at <http://www.nature.com/reprints>

Publisher’s note Springer Nature remains neutral with regard to jurisdictional claims in published maps and institutional affiliations.



Open Access This article is licensed under a Creative Commons Attribution 4.0 International License, which permits use, sharing, adaptation, distribution and reproduction in any medium or format, as long as you give appropriate credit to the original author(s) and the source, provide a link to the Creative Commons license, and indicate if changes were made. The images or other third party material in this article are included in the article’s Creative Commons license, unless indicated otherwise in a credit line to the material. If material is not included in the article’s Creative Commons license and your intended use is not permitted by statutory regulation or exceeds the permitted use, you will need to obtain permission directly from the copyright holder. To view a copy of this license, visit <http://creativecommons.org/licenses/by/4.0/>.

© The Author(s) 2021